Electronic Supplementary Material (ESI)

Design of Electrochemiluminescence Detection System through the Regulation of Charge Density in Microchannel

Yanling Huang,[a] Yilei Lu,[a] Xiaobin Huang,[a] Jian Wang,[a] Bin Qiu,[a] Fang Luo,*[ab] Zhenyu Lin*[a]

This PDF file includes:

Fig. S1-S5

Movies S1-S8

Table S1

*Corresponding author.

Email: zylin@fzu.edu.cn (Zhenyu Lin). luofang@fzu.edu.cn (Fang Luo).

S1. Chemicals

Commercial quartz glass capillaries with an outer diameter of 1.50 mm and an inner diameter of 0.86 mm were purchased from Sutter (America). Rhodamine B, 20 × PBS buffer (pH 8.0) containing NaH_2PO_4 (200 mM) and Na_2HPO_4 (200 mM) were supplied by Sangon (Shanghai, China). Ochratoxin A (OTA), aflatoxin B1 (AFB1), aflatoxin B2 (AFB2), aflatoxin G1 (AFG1) and aflatoxin G1 (AFG2) were supplied by Pribolab (Beijing, China). Dimethyl sulfoxide (DMSO), ethanol (C_2H_5OH), acetone (CH_3COCH_3), tris (hydroxymethyl) aminomethane (Tris), potassium chloride (KCl), magnesium chloridehexahydrate ($MgCl_2 \cdot 6H_2O$), sodium chloride (NaCl) and ammonium persulfate ($(NH_4)_2S_2O_8$) were purchased from Sinopharm (Shanghai, China). 7-hydroxycoumarin and 5-carboxyfluorescein were obtained from Aladdin (Shanghai, China). 1-ethyl-3-(3'-dimethylaminopropyl) carbodiimide (EDC), N-hydroxysuccinimide (NHS), 3-aminopropyltriethoxysilane (APTES), succinic anhydride (SA), dichlorotris(1,10-phenanthroline)ruthenium(II) hydrate ($Ru(phen)_3Cl_2$) and tripropylamine (TPrA) were obtained from Sigma Aldrich (Shanghai, China). All the chemicals were of analytical grade. All the solutions were prepared with deionized water (Milli-Q, Millipore, 18.2 MΩ·cm).

Capture DNA (cDNA, 5'-NH_2 TTT TTT ACA CGT GCC CAA C-3') and AFB1 aptamer (5'-GTT GGG CAC GTG TTG TCT CTC TGT GTC TCG TGC CCT TCG CTA-3') were supplied by Sangon (Shanghai, China). DNA dry powder was dissolved in B2 buffer (pH 7.5) containing Tris (10 mM), NaCl (50 mM), $MgCl_2$ (10 mM), KCl (10 mM).

S2. Apparatus and Instruments

The quartz glasses capillaries were pulled by micropipette puller (P-2000g, Sutter). The fabricated microchannels were polished by pipet micro forge (MF-900, Narishige) and each microchannel was checked by optical microscopy for the consistency of the pore size.

ECL detection was performed on lab-build system including an electrochemical workstation (CHI 660D, CH Instruments) and a BPCL Ultra-Weak Luminescence Analyzer (Institute of Biophysics, Chinese Academy of Science). For this study, a three-electrode system containing a glass carbon electrode (GCE, 3 mm in diameter), a platinum (Pt) electrode (0.5 mm in diameter) and an Ag/AgCl electrode (3 M KCl) was used in microchannel-based ECL system of this work. GCE and Pt electrode were separately situated in two reservoirs which were linked by a microchannel. $Ru(phen)_3^{2+}$/TPrA system was used as model ECL reporting system in current work. Confocal laser scanning microscopy (CLSM) images were performed on an Olympus FV1000-IX81 CLSM and a Leica TCS SP confocal system (Leica, Germany).

S3. Generation of platform current

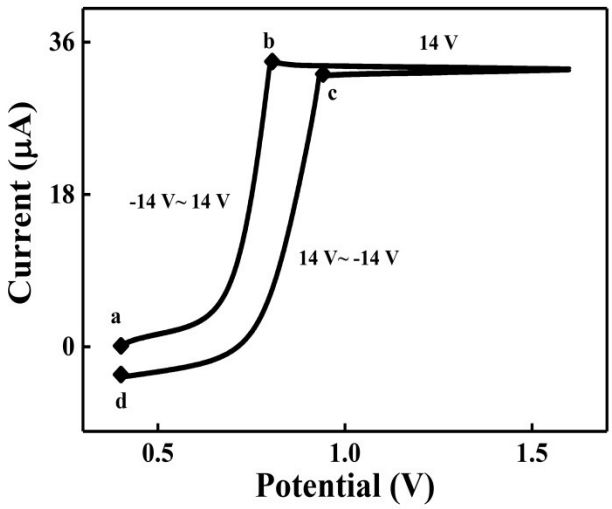

Fig. S1 The I-V curve of microchannel-based ECL sensor. Ionic current was recorded by scanning the voltage from 0.4 to 1.6 V. The functionalized microchannels were immersed into bulk solution containing Tris (10 mM), KCl (0.6 M), $Ru(phen)_3^{2+}$ (5 μM) and TPrA (13 mM). The three-electrode system consisted of a GCE (3 mm in diameter), a Pt electrode (0.5 mm in diameter) and an Ag/AgCl electrode (3 M KCl).

In ionic current rectification system, one Ag/AgCl electrode was inserted into microchannel and served as the working electrode, and another Ag/AgCl electrode was placed in external electrolyte bath to acted as the auxiliary/reference electrode. The applied potential between the working electrode and counter electrode was equal to the setting value, and ionic current increased with the increase of applied potential. For microchannel-based ECL system in this approach, E_{total} (the total potential applied by workstation) dropped at the terminals of the microchannel, so the partial potential applied on GCE (vs Ag/AgCl) was lower than the setting potential. And the electrochemical workstation automatically adjusted this lowness to equality, which however could not be achieved when the applied potential between GCE and Pt electrode reached a maximum value (14 V, in

this system) and platform current was observed. In addition, most of the ECL emission occurred at platform current region. Hence, the ECL output was mainly regulated by ionic current which corresponded to the effective radius and charge density of the functionalized microchannels.

S4. Verification for the generation of EOF and the effect of EOF on ion distribution on the tip of microchannel by synchronous electrochemical and optical experiments

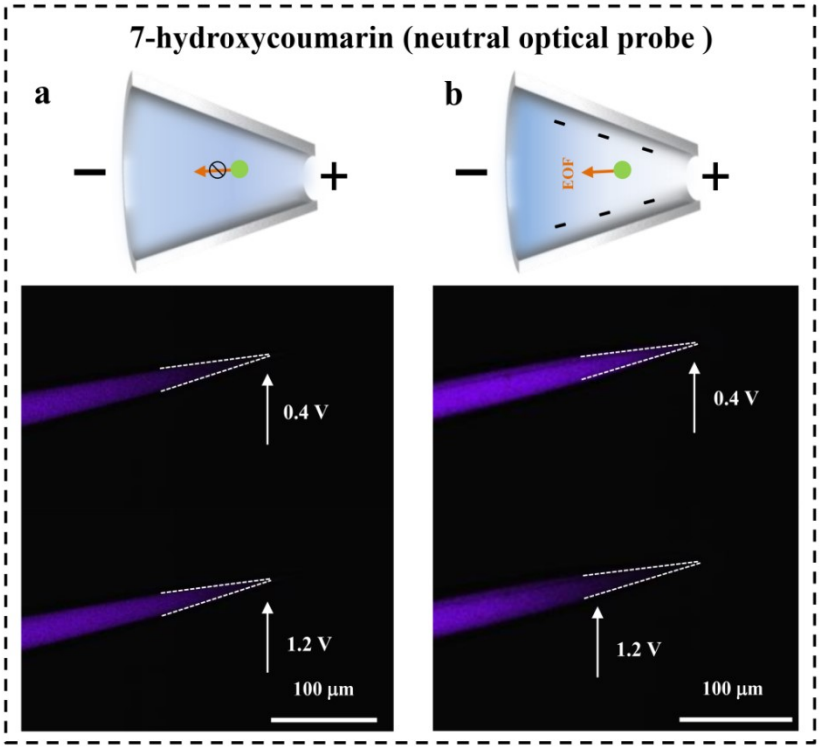

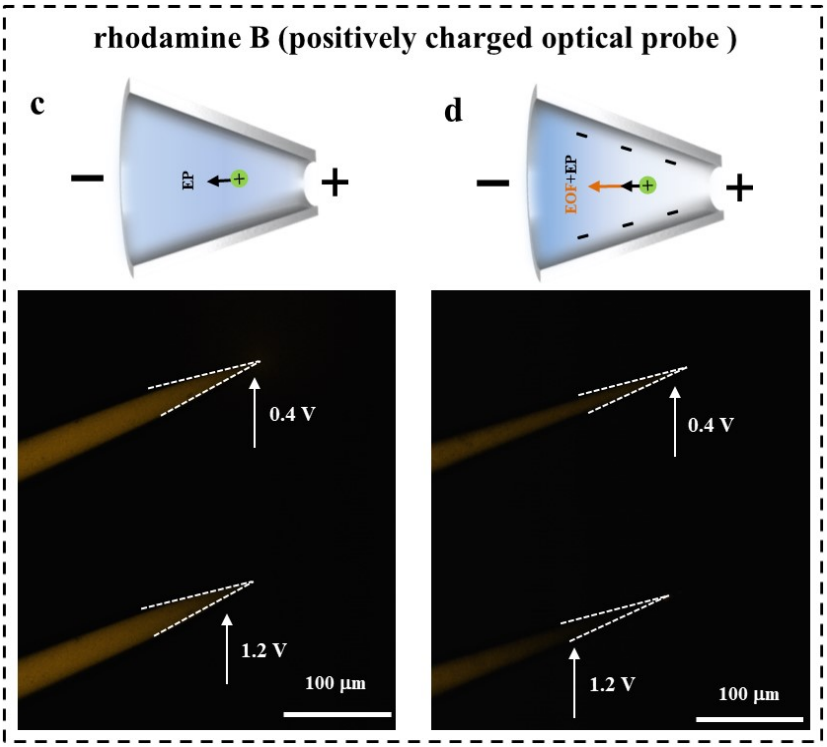

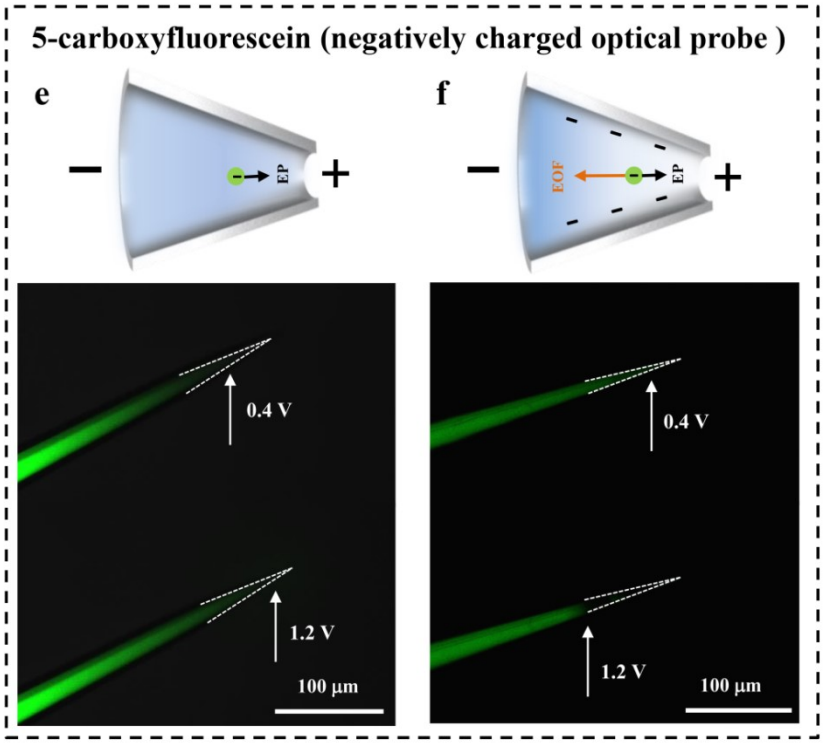

Fig. S2 Dark field fluorescence images was obtained by scanning the potential (vs Ag/AgCl) from 0.4 to 1.6 V. (a) Bare microchannel and (b) negatively charged microchannel were backfilled with bulk solution containing KCl (0.6 M) and 7-hydroxycoumarin (neutral optical probe, 10 μM). (c) Bare microchannel and (d) negatively charged microchannel were backfilled with bulk solution containing KCl (0.6 M) and rhodamine B (positively charged optical probe, 10 μM). (e) Bare microchannel and (f) negatively charged microchannel were backfilled with bulk solution containing KCl (0.6 M) and 5-carboxyfluorescein (negatively charged optical probe, 10 μM). EP and EOF represent electrophoretic and electroosmotic flow, respectively. The arrows represent the dividing line between the bright and dark areas of the fluorescent emission.

An *in-situ* confocal laser scanning microscope was employed to study the influence of negative charge density on ionic current. The mechanism verification mainly consisted of the generation of EOF and the effect of EOF on ionic distribution on tip of the

microchannel. The cyclic voltammetry scanning was applied to trigger the directional motion of ions/molecules in the microchannel. The motion direction of the 7-hydroxycoumarin molecules (neutral optical probe) in the microchannel presented the flow direction of fluid. As the initial potential set to 0.4 V, the potential drop between two terminals of the microchannel could not drive the motion of 7-hydroxycoumarin molecules. 7-hydroxycoumarin was uniformly distributed in bare or negatively charged microchannel. Under ultraviolet irradiation, there was a strong fluorescence emission occurring at all regions of the microchannel. As the potential increased, the brightest pixel in the frame of 7-hydroxycoumarin molecules fluorescence emission successively shifted from tip to base of the negatively charged microchannel (**Fig. S2b, Movie S2**). However, fluorescence emission kept unchanged in bare microchannel (**Fig. S2a, Movie S1**). The result demonstrated that EOF generated from tip to base of the negatively charged microchannel.

To visually observe the influence of EOF on ionic motion direction and ionic distribution on tip of microchannel, positively charged rhodamine B and negatively charged 5-carboxyfluorescein were adopted to present cation and anion, respectively, and then the charged optical probes were added into the bare microchannel and negatively charged microchannel, respectively. There was a strong fluorescence emission occurring at all regions of the microchannel at the initial potential of 0.4 V. As the potential increased, rhodamine B molecules migrated rapidly from tip to base by the synergistic driving of EP and EOF in the negatively charged microchannels (**Fig. S2d, Movie S4**). However, the motion of rhodamine B molecules from tip to base in bare microchannel was slow as it was driven only by EP (**Fig. S2c, Movie S3**). Compared with bare microchannel, a weaker

fluorescence emission on the tip of microchannel was obtained at negatively charged microchannel. These results demonstrated that cation was remarkably depleted on the tip of negatively charged microchannel. Backfilled into bare and negatively charged microchannels, 5-carboxyfluoresce molecules migrated from base to tip driven by EP in the bare microchannel, on the tip of which a brighter fluorescence emission was obtained (**Fig. S2e, Movie S5**). Fluorescence emission became weaker in negatively charged microchannel because 5-carboxyfluoresce migrated from tip to base driven by EP and EOF, while the EOF contradicted the EP and prevailed in ionic transport (**Fig. S2f, Movie S6**). These results indicated that anion was also depleted on the tip of microchannel in the presence of EOF. In summary, the EOF generated from tip to the base in negatively charged microchannel, thus resulting in depletion of both cations and anions on the tip of charged microchannels, which further caused the decrease of ionic current.[1]

S5. The effect of half cone angle of microchannel on EOF

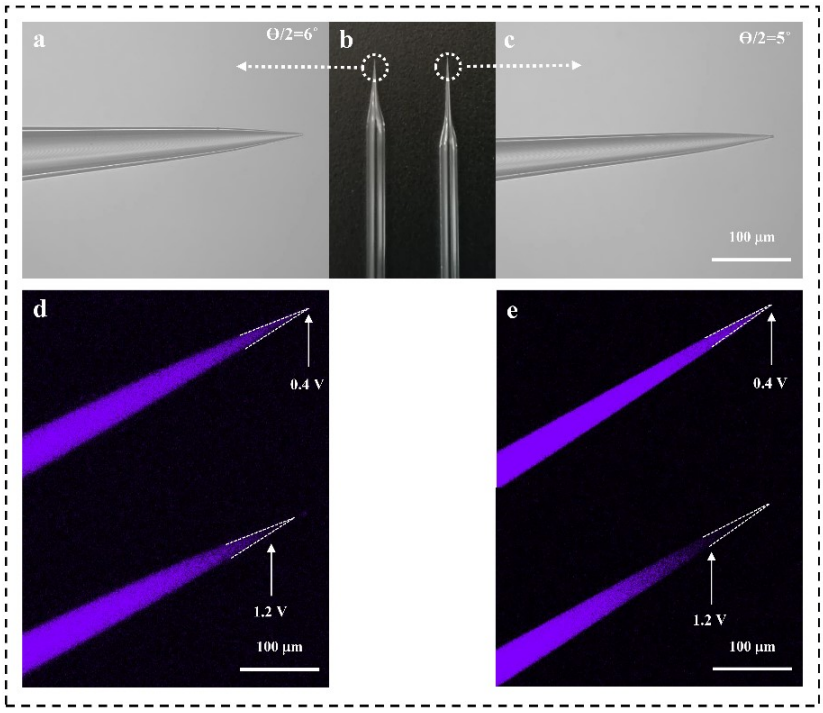

Fig. S3 The effect of microchannel cone angle on EOF. (a, c) The size-view of the fabricated microchannels with different cone angles. (b) The picture of the fabricated conical microchannel. Dark field fluorescence images were obtained by scanning the potential (vs Ag/AgCl) from 0.4 to 1.6 V. (d) Negatively charged microchannel with the half cone angle of 6˚ was backfilled with bulk solution containing KCl (0.6 M) and 7-hydroxycoumarin (neutral optical probe, 10 μM). (e) Negatively charged microchannel with the half cone angle of 5˚ was backfilled with bulk solution containing KCl (0.6 M) and 7-hydroxycoumarin (neutral optical probe, 10 μM). The arrows represent the dividing line between the bright and dark areas of the fluorescent emission.

Conical glass microchannels with half cone angle of 5˚ and 6˚ were fabricated separately. An *in-situ* confocal laser scanning microscope was employed to study the influence of half cone angle of microchannel on EOF (**Fig. S3**). The cyclic voltammetry

scanning was applied to trigger the directional motion of 7-hydroxycoumarin molecules (neutral optical probe) in the microchannel. The motion direction of 7-hydroxycoumarin molecules presented the flow direction EOF. Under the driving of external electrical field, the fluorescence emission of 7-hydroxycoumarin molecules shifted from tip to base of the negatively charged microchannels, and the fluorescence emission of 7-hydroxycoumarin molecules on tip of microchannel with the half cone angle of 5˚ was weaker than that of 6˚ (**Fig. S3d-S3e, Movie S7-S8**). The possible reason for this change was that the effective cone length of microchannel which can regulate ion migration became shorter with the increase of half cone angle. These results demonstrated that EOF occurred at the microchannel with different cone angles, and the strength of EOF in microchannel with the half cone angle of 5˚ was stronger than that of 6˚. Therefore, the microchannel with the half cone angle of 5˚ was used in this work.

S6. Optimization of the experimental parameters

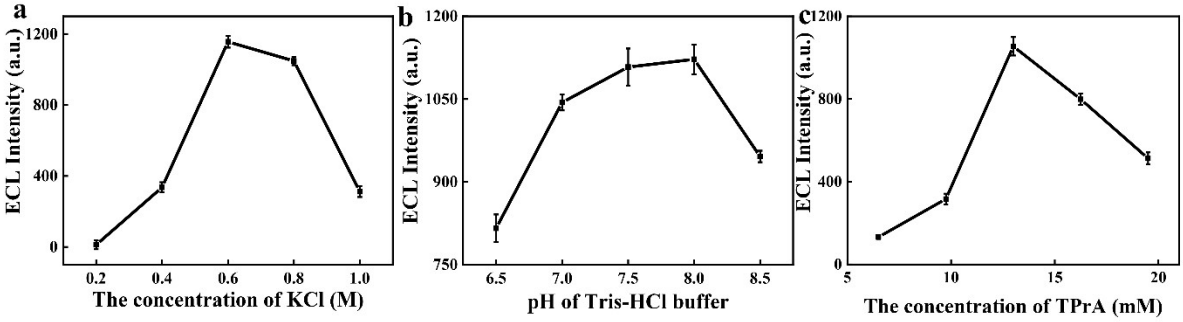

Fig. S4 The effect of the concentration of KCl, (b) the pH of Tris-HCl, and (c) the concentration of TPrA on ECL intensity. The concentrations of KCl were 0.2, 0.4, 0.6, 0.8, and 1.0 M. The pH values of Tris-HCl buffer were 6.5, 7.0, 7.5, 8.0 and 8.5. The bulk solution contained Tris (10 mM), KCl (0.6 M) solution, $Ru(phen)_3^{2+}$ (5 μM) and TPrA (13 mM). The three-electrode system consisted of a GCE (3 mm in diameter), a Pt electrode (0.5 mm in diameter) and an Ag/AgCl electrode (3 M KCl).

Various experimental parameters, such as KCl concentration, pH of Tris-HCl buffer and TPrA concentration, were optimized to achieve the best sensing performance of the proposed microchannel-based ECL system. **Fig. S4a** shows the change of ECL intensity as a function of KCl concentration. ECL intensity enhanced with the increase of KCl concentration and reached a maximum value at 0.6 M and decreased gradually with higher KCl concentration. Therefore, 0.6 M was selected as the optimized KCl concentration in the further assay. The solution pH had an effect not only on charge density of microchannel but also on luminescence efficiency.[2] **Fig. S4b** presents the pH dependent ECL output. The prepared microchannel-based ECL biosensor was measured in KCl (0.6 M) in Tris-HCl buffer with different pH values (6.5, 7.0, 7.5, 8.0, and 8.5). The ECL intensity enhanced with the increase of pH value and reached a maximum value at pH 8.0. Then, a remarkable decrease in ECL intensity was observed as the pH value further increased. Therefore, pH

8.0 was selected in the following study. The luminous efficiency could be improved through increasing the electrochemical oxidation rate of co-reactant when the concentration of luminophore was much lower than that of the co-reactant.[3, 4] The effect of TPrA concentration on ECL intensity was optimized. As shown in **Fig. S4c**, $Ru(phen)_3^{2+}$/TPrA system had a maximum ECL emission when the concentration value was 13 mM, which therefore was selected as the optimized TPrA concentration.

S7. "Negative charge density decrease" microchannel-based ECL sensor for AFB1 detection

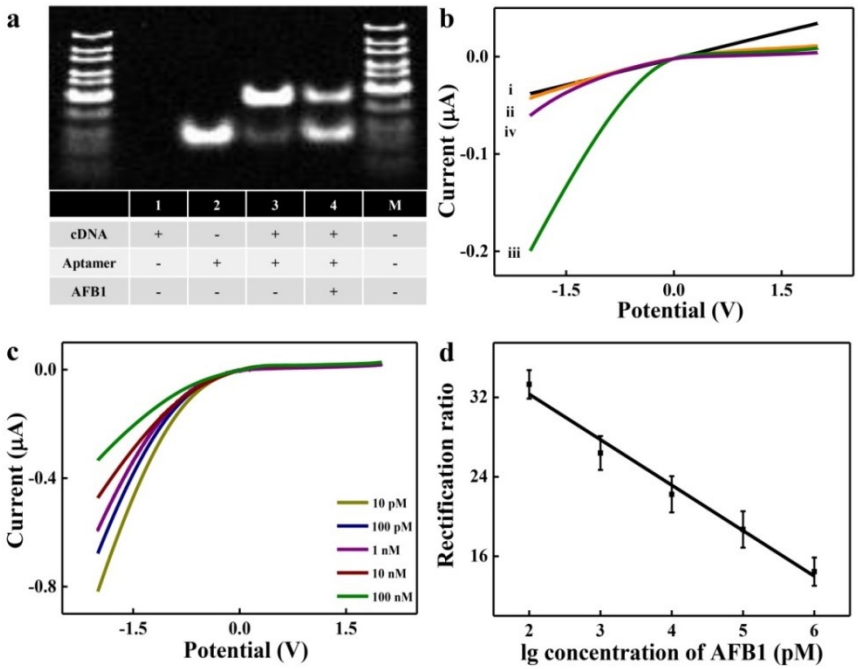

Fig. S5 Gel electrophoresis verification for the reasonable designation of nucleic acid. Lane M: DNA size marker. Lanes (1–4): cDNA, AFB1 aptamer, cDNA/aptamer complex, AFB1 + cDNA/aptamer complex, respectively. (b) The ionic current rectification of different recognition units functionalized microchannel, from i to iv: bare microchannel, carboxyl modified microchannel, aptamer/cDNA/carboxyl modified microchannel, AFB1 + aptamer/cDNA/carboxyl modified microchannel. (c) Ionic current rectification and (d) calibration curves were obtained by immersing aptamer/cDNA/carboxyl functionalized microchannel into AFB1 solution with different concentrations: 10 pM, 100 pM, 1 nM, 10 nM and 100 nM, respectively. Ionic current rectification was obtained by immersing functionalized microchannel into KCl (10 mM) solution with a pair of Ag/AgCl acted as the driving electrodes.

To verify the reasonable designation of nucleic acid, polyacrylamide gel electrophoresis (20%) experiments were carried out. As shown in **Fig. S5a**, the bands of lanes (1-4) represented cDNA, AFB1 aptamer, cDNA/aptamer complex and AFB1 + cDNA/aptamer complex, respectively. The band of cDNA/aptamer complex (lane 3) was higher than cDNA band (lane 1) and AFB1 aptamer band (lane 2), indicating that the formation of cDNA/aptamer complex with larger volume resulted in the decrease of the velocity of electrophoresis. In the presence of AFB1, AFB1 aptamer could be released from cDNA/aptamer complex. A more significant AFB1 aptamer band was observed in lane 4 compared with that in lane 3. Besides, the ionic current rectification was employed to characterize the self-assembly process in the inner surface of microchannel.[5] A linear I-V curve was obtained at bare microchannel (**curve i**) while I-V curve deviated ohmic behavior after being modified with negatively charged carboxyl groups (**curve ii**). The carboxyl modified microchannel captured cDNA/aptamer complex by EDC/NHS coupling reaction, and a similar nonlinear I-V curve with higher RR was observed (**curve iii**). RR decreased with the presence of AFB1 (**curve iv**), indicating the release of AFB1 aptamer from the inner surface of microchannel. The evolution of the dynamic RR effect after layer-by-layer modification demonstrated that different recognition units were immobilized on the inner surface of microchannel.

Table S1. AFB1 in peanut was detected by the proposed method in this work and high-performance liquid chromatography-tandem mass spectrometry (HPLC-MS/MS) (n = 6).

Sample No.	Spiked (pM)	This work			HPLC-MS/MS	
		Detected (pM)	Recovery rate (%)	RSD (%)	Detected (pM)	RSD (%)
1	0	6.81×10^{-2}	/	2.37	-	-
	1.0	1.04	97.37	3.64	-	-
	100	102.9	102.8	2.55	98.74	5.63
2	0	7.60×10^{-2}	/	3.62	-	-
	1.0	1.13	105.0	2.94	-	-
	100	96.28	96.21	4.52	95.80	5.17
3	0	8.25×10^{-2}	/	3.19	-	-
	1.0	1.07	98.85	2.61	-	-
	100	105.7	105.6	3.82	97.21	4.34

"-" represents the spiked concentration of AFB1 was lower than the limit of detection of HPLC-MS/MS method; "/" represents unknown.

Peanut was selected as the representative sample to confirm the potential application of AFB1 detection. AFB1 was extracted according to the previous method.[6] Briefly, 10 g of the peanut were grinded into peanut powder, and then 4g of which was spiked with different concentration of AFB1 and mixed in a vortex mixer. After the addition of extraction solvent (10 mL, volume ratio was 6:4, methanol/water), the samples were mixed using vortex mixer for 30 min. After being centrifugated at 6000 rpm for 10 min, the extract was passed through a syringe filter (220 nm) to remove the impurities with larger size, followed by being diluted with Tris-HCl buffer to form a finally spiked AFB1 concentration of 1 pM and 100 pM. For AFB1 detection in real sample, the following steps were the same

as that for the construction of ECL biosensor. As shown in **Table S1**, the obtained ECL output was compared with the standard curve to estimate the AFB1 concentrations in the peanut samples. The recovery rate of the AFB1 detection was in the range of 96.21 to 105.6%, and the relative standard deviation (RSD) was between 2.37 and 4.52%. To further confirm the potential application of the proposed method in real samples, HPLC-MS/MS assays were performed. The extracted sample was diluted to a finally spiked AFB1 concentration of 100 pM. Compared with the recovery rate obtained from HPLC-MS/MS, the results in our assay demonstrated that the proposed microchannel-based ECL sensor could be used for the quantification of AFB1 in the real samples.

References

1. W. Lan, D. Holden and H. White, *J. Am. Chem. Soc.*, 2011, **133**, 13300-13303.
2. Y. Zheng, S. Zhao, S. Cao, S. Cai, X. Cai and Y. Li, *Nanoscale*, 2017, **9**, 433-439.
3. X. Liu, L. Shi, W. Niu, H. Li and G. Xu, *Angew. Chem., Int. Ed.*, 2007, **119**, 425-428.
4. X. Li, Y. Li, R. Feng, D. Wu, Y. Zhang, H. Li, B. Du and Q. Wei, *Sens. Actuators, B*, 2013, **188**, 462-468.
5. K. Zhang, X. He, Y. Liu, P. Yu, J. Fei and M. L., *Anal. Chem.*, 2017, **89**, 6794-6799.
6. C. Wang, J. Qian, K. An, C. Ren, X. Lu, N. Hao, Q. Liu, H. Li, X. Huang and K. Wang, *Biosens. Bioelectron.*, 2018, **108**, 69-75.